Spatial separation of rotating binary Bose-Einstein condensates by tuning the dipolar interactions

Ramavarmaraja Kishor Kumar,[1,2,*] Lauro Tomio,[2,3,†] and Arnaldo Gammal[1,‡]
[1]*Instituto de Física, Universidade de São Paulo, 05508-090 São Paulo, Brazil*
[2]*Instituto de Física Teórica, Universidade Estadual Paulista, 01156-970 São Paulo, SP, Brazil*
[3]*Instituto Tecnológico de Aeronáutica, DCTA, 12228-900 São José dos Campos, SP, Brazil*

(Received 3 November 2018; published 4 April 2019)

We are pointing out relevant anisotropic effects, related to spatial separation and miscibility, due to dipole-dipole interactions in rotating binary dipolar Bose-Einstein condensates by considering symmetric (^{164}Dy-^{162}Dy) and asymmetric (^{168}Er-^{164}Dy, ^{164}Dy-^{87}Rb) dipolar mixtures. The binary mixtures are kept in a strong pancake-shaped trap, with repulsive two-body interactions and fixed rotation, modeled by an effective two-dimensional coupled Gross-Pitaevskii equation. The anisotropy of the dipolar interactions on miscibility and vortex-lattice structures is studied by tuning the dipole-dipole interaction (DDI) from repulsive to attractive by varying the dipole polarization angle. A clear spatial separation is verified in the densities for attractive DDI, when the inter- to intraspecies contact interaction ratio is larger than 1, being angular for symmetric mixtures and radial for asymmetric ones. The signature of hidden vortices is evidenced in the particular dipolar-symmetric case. Another relevant outcome is the observed mass-imbalance sensibility verified by the vortex-pattern binary distributions in symmetric and asymmetric-dipolar mixtures, which requires the use of a relation for nonhomogeneous mixtures to estimate the miscibility of two components.

DOI: 10.1103/PhysRevA.99.043606

I. INTRODUCTION

The realization of Bose-Einstein condensates (BEC) with chromium (^{52}Cr) atoms has opened a new research direction called dipolar quantum gases [1], allowing first experimental studies on strong dipolar effects in quantum superfluid [2]. Following these investigations with chromium, many subsequent studies have been carried out by different experimental groups on fermionic and bosonic properties of strongly dipolar ultracold gases, such as with dysprosium and erbium [3–10]. As reported recently in Ref. [11], within the realization of two-species mixtures with strongly dipolar atoms of erbium and dysprosium, novel fascinating possibilities in physics are being revealed due to the peculiar competition between isotropic short-range contact interaction and long-range anisotropic dipole-dipole interaction (DDI). The experimental production of BEC with dysprosium (^{162}Dy) has been improved due to a new technique reported in Ref. [12] which allows efficient loading from a magneto-optical trap; the ability to tune the strength of the DDI has been demonstrated in Refs. [13,14] for rotating strongly dipolar single-atom species. These highly magnetic lanthanide atoms, having strong DDIs, can present quite relevant and interesting quantum behaviors, including ferrofluidity and self-bound droplets [2,15,16]. As demonstrated in Ref. [15], the quantum fluctuations in strongly dipolar Bose gases can stabilize droplets against the mean-field collapse. (On self-bound droplets in dipolar and spinor bosonic systems, see Ref. [17] for an updated review.) Related to vortices in rotating dipolar BEC contrasting with nondipolar systems, a review is presented in Ref. [18], where the interplay of magnetism with vorticity is being explored. Apart from experimental studies, there are previous investigations on the stability of trapped dipolar BECs in Ref. [19], as well as several theoretical studies performed with dipolar mean-field theory, which are based on the construction of the corresponding pseudopotential [20,21]. The stability properties of binary dipolar mixtures with two atomic species, within a pancake-trapped symmetry, have been studied in Ref. [22]. The ferrofluidlike pattern formations are studied in Ref. [23] for two-component BECs with DDIs, and more recently, in Ref. [24] considering instabilities and patterns verified by oppositely polarized dipoles in a two-component BEC. Rotational properties of two-component dipolar BEC in concentrically coupled annular traps were also studied in Ref. [25] by assuming only one dipolar component.

Following previous studies from Refs. [26,27], the miscible-immiscible transition (MIT) of the binary dipolar mixtures with ^{162,164}Dy and ^{168}Er have been recently investigated by some of us in Refs. [28–30]. For these coupled dipolar systems, in Ref. [28] the miscible-immiscible stable conditions within a full three-dimensional (3D) formalism were established, considering repulsive contact interactions, from pancake- to cigar-type trap configurations. The rotational properties and vortex-lattice structures were further investigated in Ref. [29]. More recently, in Ref. [30], with the binary system confined in squared optical lattices, the effect of changing the inter- to intraspecies scattering length was investigated. Among the observed characteristics of these strong dipolar binary systems, relevant for further investigations are the possibilities to alter the effective time-averaged DDI from repulsive to attractive by tuning the polarization angles of both interacting dipoles.

*kishor.bec@gmail.com
†lauro.tomio@unesp.br
‡gammal@if.usp.br

Motivated by the above previous studies, considering that the interplay between DDIs and contact interactions can bring us different interesting effects in the MIT, showing richer vortex-lattice structures in rotating binary dipolar systems, in the present work we investigate properties of strong dipolar mixtures in a two-dimensional (2D) rotating magnetic trap by tuning the polarization angles of the dipoles together with the contact interspecies interactions. Within our aim, we explore symmetric- and nonsymmetric-dipolar coupled mixtures in a regime where the system is stable for positive and negative DDIs. The nondipolar case is also verified at a critical polarization angle. By assuming fixed the rotation frequency and trap aspect ratio, the interactions can be controlled by two independent ways: With Feshbach resonance techniques [31] one can alter the two-body contact interactions (see Ref. [32], for a detailed review on the applications of these techniques to ultracold gases and mixed atomic species); and by external magnetic fields one can tune the polarization angles of the dipoles such that the DDI can be changed from repulsive to attractive [33]. The stability of dipolar BEC affected by the attractive part of the DDI can be kept by using a strong axially confining pancake-shaped trap with suitable repulsive contact interactions. Peculiar nontrivial behaviors are expected in the density distributions, for dipolar-symmetric mixtures such as ^{164}Dy-^{162}Dy, in comparison with the nonsymmetric ones such as ^{168}Er-^{164}Dy and ^{164}Dy-^{87}Rb, due to their distinct miscibility properties. Therefore, due to actual possibilities for experimental investigations [7,11], we select these systems as the main focus of our analysis.

Next we present the basic formalism and notation followed by a section with our main results for the three kinds of dipolar mixtures we consider. In a final section, we have a summary with our main conclusions.

II. FORMALISM AND PARAMETRIZATION

The coupled dipolar system with condensed two atomic species are assumed to be confined in strongly pancake-shaped harmonic traps, with fixed aspect ratios, such that $\lambda_i = \omega_{i,z}/\omega_{i,\perp} = 20$ for both species $i = 1, 2$, where $\omega_{i,z}$ and $\omega_{i,\perp}$ are, respectively, the longitudinal and transverse trap frequencies. The coupled Gross-Pitaevskii (GP) equation is cast in a dimensionless format, with energy and length units given, respectively, by $\hbar\omega_{1,\perp}$ and $l_\perp \equiv \sqrt{\hbar/(m_1\omega_{1,\perp})}$, where $\omega_{1,\perp} \equiv \omega_1$ is the transverse frequency, with m_1 the mass, for the species $i = 1$. Correspondingly, the space and time variables are given in units of $l_\perp$ and $1/\omega_1$, respectively, such that $\mathbf{r} \to l_\perp \mathbf{r}$ and $t \to \tau/\omega_1$. Within these units and by adjusting both trap frequencies such that $m_2\omega_{2,\perp}^2 = m_1\omega_{1,\perp}^2$, the dimensionless external 3D trap potential for both species can be written as

$$V_{3D}(\mathbf{r}) = \tfrac{1}{2}(x^2 + y^2 + \lambda^2 z^2) \equiv V(x, y) + \tfrac{1}{2}\lambda^2 z^2. \quad (1)$$

In the case of the DDI, we consider that one of the atoms (A_i) is at position $\mathbf{r}$ with the other one (A_j) at position $\mathbf{r}'$, respectively, with their line vector $\mathbf{r} - \mathbf{r}'$ making an angle θ related to the z axis such that $\theta \approx 90^\circ$ for a strong pancake-shaped trap, as given by Eq. (1) (each of the atoms can be of species $i, j = 1, 2$). Next, we assume both dipoles are polarized in the same direction, making an angle φ with respect to the z axis. See the corresponding illustration in Fig. 1. The tunability is performed by using time-dependent magnetic fields with dipoles rapidly rotating around the z axis [33,34]. The magnetic field is given by the combination of a static part along the z direction and a fast rotating part in the (x, y) plane, having a frequency such that the atoms are not significantly moving during each period. Having once performed a time averaging of the DDI within a period, the corresponding 3D averaged interaction between the coupled dipolar species i and j, with their respective magnetic dipole moments μ_i and μ_j given in terms of the Bohr magneton μ_B, can be written in our dimensionless format as [33]

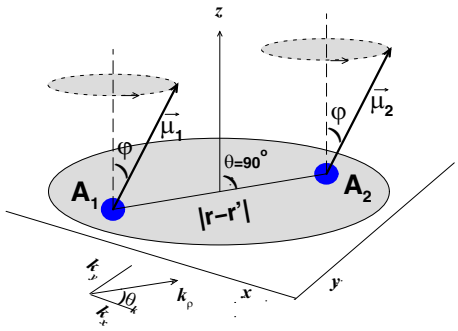

FIG. 1. An illustration of the DDI between the two atomic species 1 and 2, given in coordinate space, where the polarization angle is φ, with the assumption that both atoms are in the (x, y) plane ($\theta = 90^o$).

$$\left\langle V_{3D}^{(d)}(\mathbf{r} - \mathbf{r}')\right\rangle_{ij} = \frac{\mu_0\mu_i\mu_j}{\hbar\omega_1 l_\perp^3}\frac{1 - 3\cos^2\theta}{|\mathbf{r} - \mathbf{r}'|^3}\left(\frac{3\cos^2\varphi - 1}{2}\right), \quad (2)$$

where μ_0 is the free-space permeability. In the following, we assume $\theta = 90^\circ$, such that the DDI strength is repulsive for $\varphi < \varphi_M$ and attractive when $\varphi > \varphi_M$ (where $\varphi_M \approx 54.7^\circ$ is the so-called "magic angle," when the DDI is averaged to zero). The factor within parenthesis in Eq. (2) results from the time-averaging procedure on the dipole orientation around the z axis. Large values for the aspect ratios λ_i allow us to reduce the original 3D formalism to 2D by considering the usual factorization of the 3D wave function in two components given by $\psi_i(x, y, \tau)\chi_i(z)$, where $\chi_i(z) \equiv (\lambda_i/\pi)^{1/4}e^{-\lambda_i z^2/2}$. In this case, the ground-state energy for the harmonic trap in the z direction is a constant factor to be added in the total energy. It is safe to assume a common mass-independent transversal wave function for both components with $\lambda_i = \lambda$, as any mass asymmetry can be absorbed by changing the corresponding aspect ratio. This approach for the reduction to 2D implies that we also need to alter the nonlinear parameters accordingly, as the integration on the z direction will bring us a λ dependence in the nonlinear parameters. So, the two-body contact interactions related to the scattering lengths a_{ij}, as well as the dipole-dipole interaction parameters for the species $i, j = 1, 2$, are defined as [29]

$$g_{ij} \equiv \sqrt{2\pi\lambda}\frac{m_1 a_{ij} N_j}{m_{ij} l_\perp}, \quad d_{ij} = \frac{N_j}{4\pi}\frac{\mu_0\mu_i\mu_j}{\hbar\omega_1 l_\perp^3},$$
$$a_{ii}^{(d)} \equiv \frac{1}{12\pi}\frac{m_i}{m_1}\frac{\mu_0\mu_i^2}{\hbar\omega_1 l_\perp^2}, \quad a_{12}^{(d)} = a_{21}^{(d)} = \frac{1}{12\pi}\frac{\mu_0\mu_1\mu_2}{\hbar\omega_1 l_\perp^2}, \quad (3)$$

where $N_{j=1,2}$ is the number of atoms of species j and $m_{ij} = m_i m_j/(m_i + m_j)$ is the reduced mass. For the dipolar parameters, we have valid the general relation $d_{12}d_{21} = d_{11}d_{22}$. In the next, the length unit will be adjusted to $l_\perp = 1\mu\text{m} \approx 1.89 \times 10^4 a_0$, where a_0 is the Bohr radius, such that a_{ij} and $a_{ij}^{(d)}$ can be conveniently given in terms of a_0 in our numerical analysis.

With the above notations for units and parameters, the corresponding coupled GP equation in 2D is given by

$$i\frac{\partial\psi_i}{\partial\tau} = \left[\frac{-m_1}{2m_i}\left(\frac{\partial^2}{\partial x^2}+\frac{\partial^2}{\partial y^2}\right)+V(x,y)-\Omega L_z+\sum_{j=1,2} g_{ij}|\psi_j|^2 + \sum_{j=1,2} d_{ij}\int_{-\infty}^{\infty} dx'dy'V^{(d)}(x-x',y-y')|\psi_j'|^2\right]\psi_i, \tag{4}$$

where $V^{(d)}(x,y)$ is the reduced 2D expression for the DDI, and $\psi_i \equiv \psi_i(x,y,\tau)$ and $\psi_i' \equiv \psi_i(x',y',\tau)$ are the components of the total 2D wave function, normalized to 1, $\int_{-\infty}^{\infty} dxdy|\psi_i|^2 = 1$. L_z is the angular momentum operator with Ω the corresponding rotation parameter (in units of ω_1), which is common for the two components. The external potential provided by the harmonic trap is given by $V(x,y) = \frac{1}{2}(x^2+y^2)$.

In 2D momentum space, the DDI can be expressed as the combination of two terms, considering the orientations of the dipoles φ and projection of the Fourier transformed of $V^{(d)}(x,y)$ in momentum space. One term perpendicular with the other parallel to the direction of the dipole inclinations, respectively, is given by [26,27]

$$\widetilde{V}_\perp^{(d)}(k_x,k_y) = 2 - 3\sqrt{\frac{\pi}{2\lambda}}k_\rho \exp\left(\frac{k_\rho^2}{2\lambda}\right)\text{erfc}\left(\frac{k_\rho}{\sqrt{2\lambda}}\right) \tag{5}$$

and

$$\widetilde{V}_\parallel^{(d)}(k_x,k_y) = -1 + 3\frac{k_x^2}{k_\rho}\sqrt{\frac{\pi}{2\lambda}}\exp\left(\frac{k_\rho^2}{2\lambda}\right)\text{erfc}\left(\frac{k_\rho}{\sqrt{2\lambda}}\right), \tag{6}$$

where $k_\rho^2 \equiv k_x^2 + k_y^2$, with $\text{erfc}(x)$ being the complementary error function of x. The k_x explicit in the right-hand side of the above parallel term is the projected wave number in the (x,y) plane in the direction of the polarization tilt, which was arbitrarily assumed in the x axis when that term was derived [26]. Generalizing the description to a polarization field rotating in the (x,y) plane, as $\mathbf{k}_\rho = (k_x,k_y) = (k_\rho\cos\theta_k, k_\rho\sin\theta_k)$ and all directions θ_k are equally possible, we should average $k_\rho^2\cos^2\theta_k$ in the plane such that k_x^2 should be replaced by $k_\rho^2/2$ in the parallel term shown in Eq. (6). By combining the two terms according to the dipole orientations φ, the total 2D momentum-space DDI can be written as

$$\widetilde{V}^{(d)}(k_x,k_y) = \frac{3\cos^2\varphi - 1}{2}\widetilde{V}_\perp^{(d)}(k_x,k_y) \equiv V_\varphi(k_\rho). \tag{7}$$

The 2D configuration-space effective DDI is obtained by applying the convolution theorem in Eq. (4), performing the inverse 2D Fourier transform for the product of the DDI and density, such that $\int dx'dy'V^{(d)}(x-x',y-y')|\psi_j'|^2 = \mathcal{F}_{2D}^{-1}[\widetilde{V}^{(d)}(k_x,k_y)\widetilde{n}_j(k_x,k_y)]$. From Eqs. (5)–(7), one should notice that such momentum-space Fourier transform of the dipole-dipole potential is changing the sign at some particular large momentum k_ρ. However, after applying the convolution theorem with the inverse Fourier transform (by integrating the momentum variables), the corresponding coordinate-space interaction has a definite value, as in the 3D case, which is positive for $\varphi \leqslant \varphi_M$ and negative for $90^\circ \geqslant \varphi > \varphi_M$. For larger angles, when the DDI is predominantly attractive, close to $\varphi \approx 90^\circ$, the system can become unstable, requiring enough repulsive contact interactions and a suitable strong pancake-shaped trap. In view of these requirements, in order to stabilize the binary dipolar rotating system also in this extreme dipolar condition, along this work we have assumed a quite strong aspect ratio λ for the trap, combined with enough large contact interactions. Therefore, to explore anisotropic dipolar effects, by increasing the angle φ from zero to larger values we can provide attractive interactions between dipoles, with the inter- and intraspecies dipolar interactions being equally affected.

Parametrization. For the three various coupled dipolar systems that we are investigating, the corresponding magnetic dipole moments of the species are the following: $\mu = 10\mu_B$ for ^{162,164}Dy, $\mu = 7\mu_B$ for ^{168}Er, and $\mu = 1\mu_B$ for ^{87}Rb. So, by considering the definitions given in (3), the strengths of the DDI are $a_{ij}^{(d)} = 131\,a_0$ $(i,j=1,2)$ for the symmetric-dipolar mixture ^{164}Dy-^{162}Dy, and $a_{11}^{(d)} = 66\,a_0$, $a_{22}^{(d)} = 131\,a_0$ and $a_{12}^{(d)} = a_{21}^{(d)} = 94\,a_0$, for the ^{168}Er-^{164}Dy mixture. As the magnetic moment of ^{87}Rb is negligible in comparison with the ^{164}Dy, we assume the binary mixture ^{164}Dy-^{87}Rb as being single-species dipolar, such that $a_{22}^{(d)} = a_{12}^{(d)} \approx 0$. In all the cases, we assume the number of atoms for both species are identical and fixed at $N_1 = N_2 = 10^4$. For a symmetric-dipolar mixture ($\mu_1 = \mu_2$) we have $d_{12} = d_{11} = d_{22}$.

In the case of contact interactions, we should consider enough large repulsive scattering lengths in view of our stability requirements. However, the typical values of the intraspecies contact interactions [such as $a_s \approx 92(8)a_0$ for ^{164}Dy$_2$ and $a_s \approx 200(23)a_0$ for ^{164}Er$_2$] may be too large, such that they can suppress the dipolar effects. So, it being known that these two-body interactions can be adjusted by applying Feshbach resonance mechanisms [31,32], we found it appropriate to fix both intraspecies contact interactions at $a_{11} = a_{22} = 50a_0$, allowing the interspecies one to be explored from smaller to larger values through the ratio parameter $\delta \equiv a_{12}/a_{11}$.

From previous studies related to vortex-pattern structures, this parameter is associated to a first-order MIT for uniform coupled condensed mixtures, which should be replaced by a second-order one for nonuniform mixtures, as discussed in the next section.

Having once selected the polarization angle and δ as the appropriate parameters to alter the miscibility properties of a mixture, we fix the other parameters guided by possible realistic settings and stability requirements. For the rotation frequency parameter, we choose $\Omega = 0.6$, as we found that $\Omega < 0.4$ may not be appropriate to observe vortex-lattice structures. For the harmonic trap potential, we assume a strong pancake-shaped trap in the (x,y) plane, with an aspect ratio $\lambda = 20$. Given the transversal trap frequency for the first species as $\omega_1 = 2\pi \times 60\ \text{s}^{-1}$, the trap frequencies for the

second species can be found from our assumption on the angular frequencies such that $m_2\omega_2^2 \simeq m_1\omega_1^2$, implying that the trap frequencies are about the same for both species in the cases of ^{164}Dy-^{162}Dy and ^{168}Er-^{164}Dy binary mixtures, whereas for the ^{164}Dy-^{87}Rb the trap frequency of the rubidium is $\omega_2 \approx 2\pi \times 82\ \ \mathrm{s}^{-1}$.

Numerical procedure. In order to solve the GP formalism given by the coupled Eq. (4), the numerical approach applied is based on the split-step Crank-Nicolson method [35,36], combined with a standard method for evaluating DDI integrals in the momentum space (see details in Ref. [29] and references therein). In the search for stable solutions, the numerical simulations were carried out in imaginary time on a grid with a maximum of 528 points in both $x-y$ directions, with spatial and time steps $\Delta x = \Delta y = 0.05$ and $\Delta t = 0.0005$, respectively. Both wave-function components are renormalized to one at each time step. By looking for stationary vortex states, we solve Eq. (4) with different initial conditions. In view of previous tests on the initial suitable conditions, we use a combination of angular harmonics followed by convergence tests of the solutions for the given inputs, within a procedure also discussed in Ref. [29].

III. MISCIBILITY OF BINARY DIPOLAR MIXTURES

A relevant property that strongly affects the vortex patterns of a coupled binary mixture is miscibility, which has been shown to vary according to the inter- and intraspecies interactions. As demonstrated in Ref. [37] for nondipolar systems, the accepted condition for phase separation is based on the consideration of minimizing the interaction energy such that the relation between the two-body scattering lengths (assumed to be positive) $a_{12} > \sqrt{a_{11}a_{22}}$ is satisfied when the coupled system becomes immiscible, with the equality establishing a first-order miscible-immiscible transition. In terms of the contact parameters g_{ij} defined in Eq. (3), a mass factor should appear. However, the condition for nondipolar MIT $\delta = a_{12}/\sqrt{a_{11}a_{22}}$ was derived for a homogeneous dipolar mixture assuming $m_1 = m_2$ and $N_1 = N_2$ such that we can also write it as $\delta = g_{12}/\sqrt{g_{11}g_{22}}$.

By considering homogeneous dipolar mixtures in a general 3D system, this condition was generalized in Ref. [28] by replacing the contact parameters with the corresponding ones that include the dipolar interaction strengths d_{ij}. In the present case, with the definitions given in Eq. (3) and with the DDI angular factor obtained in Eq. (7), $f(\varphi) \equiv 4\pi(3\cos^2\varphi - 1)$, the corresponding critical condition for MIT for homogeneous dipolar mixture is verified at $\Delta = 0$, with Δ defined by

$$\Delta = \frac{|g_{11} + d_{11}f(\varphi)||g_{22} + d_{22}f(\varphi)|}{|g_{21} + d_{21}f(\varphi)|^2} - 1. \tag{8}$$

By applying this condition, the system is miscible for $\Delta > 0$ and immiscible for $\Delta < 0$. Also related to the above condition, one should notice that in Ref. [28], instead of the polarization angle φ, we have the angle between the wave vector $\mathbf{k}$ and the dipole moment, which is assumed close to zero in our study with a strong pancake-shaped system. We should notice that for nondipolar systems ($d_{ij} = 0$), $\Delta > 0$ corresponds to $\delta < 1$, and $\Delta < 0$ to $\delta > 1$. For symmetric-dipolar mixtures, irrespective to the angle φ, the MIT point ($\Delta = 0$) remains in the same position as that obtained for nondipolar systems, but it is modified for nonsymmetric-dipolar mixtures, having a maximal effect when one of the species is nondipolar. For pure dipolar coupled systems, under the above homogeneous condition the miscibility is not affected, as $d_{12}^2 = d_{11}d_{22}$ irrespective of being repulsive or attractive the DDI.

However, as also discussed in Ref. [38], besides the fact that it is quite useful, a relation such as (8), due to its simplicity, also carries serious limitations considering that it was derived with the assumption that the coupled condensates are uniform with the kinetic energy associated with the boundaries being neglected. By the indications that the kinetic energy should play a vital role in determining the configuration of a two-component BEC, following Ref. [38], a more general parameter was defined and studied in Ref. [28] to estimate the miscibility of a coupled dipolar system, which is given by

$$\eta \equiv \int_{-\infty}^{\infty} dxdy|\psi_1||\psi_2|. \tag{9}$$

This definition replaces the first-order homogeneous condition (8) by a second-order one, with a system being completely miscible or immiscible for the case $\eta = 1$ or 0, respectively. So, following Ref. [28], we can assume the system is almost miscible if $\eta \geqslant 0.75$, and almost immiscible if $\eta \leqslant 0.35$.

Therefore, to alter the miscibility of a dipolar coupled system, beyond the external mechanisms that can be applied to adjust the contact two-body interactions (related to the two-body s-wave scattering lengths) and polarization angle of the dipoles, one should also consider intrinsic parameters which can affect the associated kinetic energy, such as the masses of the two species. In this regard, when considering the two stronger dipolar binary cases that we are investigating, we can verify from a previous study that the symmetric ^{164}Dy$-^{162}$Dy binary mixture is more miscible than the asymmetric one, ^{168}Er$-^{164}$Dy, when we assume fixed repulsive DDI (as for $\varphi = 0$) and with $\delta < 1$ (contact interactions below the MIT point for homogeneous systems). These quite distinct properties related to the miscibility of the two coupled dipolar mixtures, verified in Ref. [28] and also observed in our following results, cannot be justified by considering only the dipole-moment differences, as the dipolar interactions, when different for both species, can only affect the relation by shifting the transition point.

In order to estimate how the kinetic-energy asymmetry due to the mass imbalance can affect the miscibility, let us consider the other parameters fixed. In this case, as shown by Eq. (4), the mass imbalance appears explicitly in the kinetic-energy terms (reflected in the second component of the coupled system), with the mass-imbalance factor $(m_1/m_2 - 1)$ being 0.0244 for ^{168}Er$-^{164}$Dy and 0.0123 for ^{164}Dy$-^{162}$Dy. This implies that the net effect in the kinetic energy due to the mass imbalance in ^{168}Er$-^{164}$Dy is about twice that obtained for ^{164}Dy$-^{162}$Dy. So the system with less mass asymmetry is the more miscible one due to the corresponding smaller asymmetry in the kinetic energy. Beyond this effect in the kinetic energy, in our approach the mass imbalance will also affect the nonlinear parametrization defined in Eq. (3), considering the given physical values we are assuming for the

quantities a_{ij} and $a_{ij}^{(d)}$. These effects due to the kinetic energy are expected to be enhanced in particular when the application of the Thomas-Fermi (TF) approximation is less valid, as when the interactions become less repulsive or attractive. As it will be shown, the mass-imbalance effect and corresponding sensitivity can also be appreciated in rotating binary dipolar mixtures by comparing the vortex-pattern results and the miscibility of the two species in the case of the dipolar-symmetric ^{164}Dy−^{162}Dy mixture. By eliminating the mass asymmetry, identical results for the vortex patterns will be obtained.

IV. RESULTS ON BINARY DIPOLAR MIXTURES

Our main results are presented in this section, for both symmetric- and asymmetric-dipolar cases, with the DDI varying from repulsive to attractive, using the dipole polarization angle, and with contact interaction ratio δ varying from 0.75 to 1.45. The other parameters, such as number of atoms for each species, trap aspect ratio, intraspecies scattering lengths, and rotation frequency, are fixed as discussed in Sec. II B.

We consider three different dipolar condensed mixtures, which have different natural characteristics with respect to their miscibility properties, when $\varphi = 0$ and the DDI is repulsive, as well as different vortex-pattern structures when the binary system is under rotation [28,29]. For the symmetric-dipolar coupled system, ^{164}Dy-^{162}Dy, our results are organized and discussed in Sec. IV A. In Sec. IV B, we present the results for the asymmetric-dipolar mixture, ^{168}Er-^{164}Dy. Finally, for comparison with the previous two cases, in (C) we also examine the ^{164}Dy-^{87}Rb case, where one of the species has negligible dipole moment.

A. The symmetric-dipolar mixture, ^{164}Dy-^{162}Dy

We first consider the nearly symmetric mixture ^{164}Dy-^{162}Dy, within our aim to analyze anisotropic properties of rotating dipolar interactions, by tuning the dipoles from $\varphi = 0^\circ$ to 90° together with variations in the relative contact interactions. In this case, both dipolar species have the same magnetic dipole moments, polarized in the same direction. Among the coupled systems we are considering, this one is known to be more miscible than the other two cases, at least when the DDI is repulsive, as for $\varphi = 0^\circ$. As verified in Ref. [29], this dipolar mixture can show triangular, squared, striped, and domain-wall vortex-lattice structures regarding the ratio between inter- and intraspecies contact interaction δ and rotation frequency Ω. The system undergoes a miscible-to-immiscible crossover at $\delta = 1$. In particular, for repulsive DDI, as verified in Fig. 2, instead of creating miscible vortices as occurs for $\delta \leqslant 1$, by increasing the interspecies interaction the two components tend to separate, forming different patterns, from striped to domain-wall structures.

Among the sets with different δ values, the more miscible one is shown in Fig. 2(A) for $\delta = 0.75$. In this case, squared-lattice structures are shown in the densities at $\varphi = 0$. As φ increases, the number of vortices gradually decreases. Some distortions are observed near $\varphi = 45^\circ$, but the square-lattice patterns are sustained up to $\varphi \approx 60^\circ$, where we are already entering in the attractive regime of the DDI [see panels

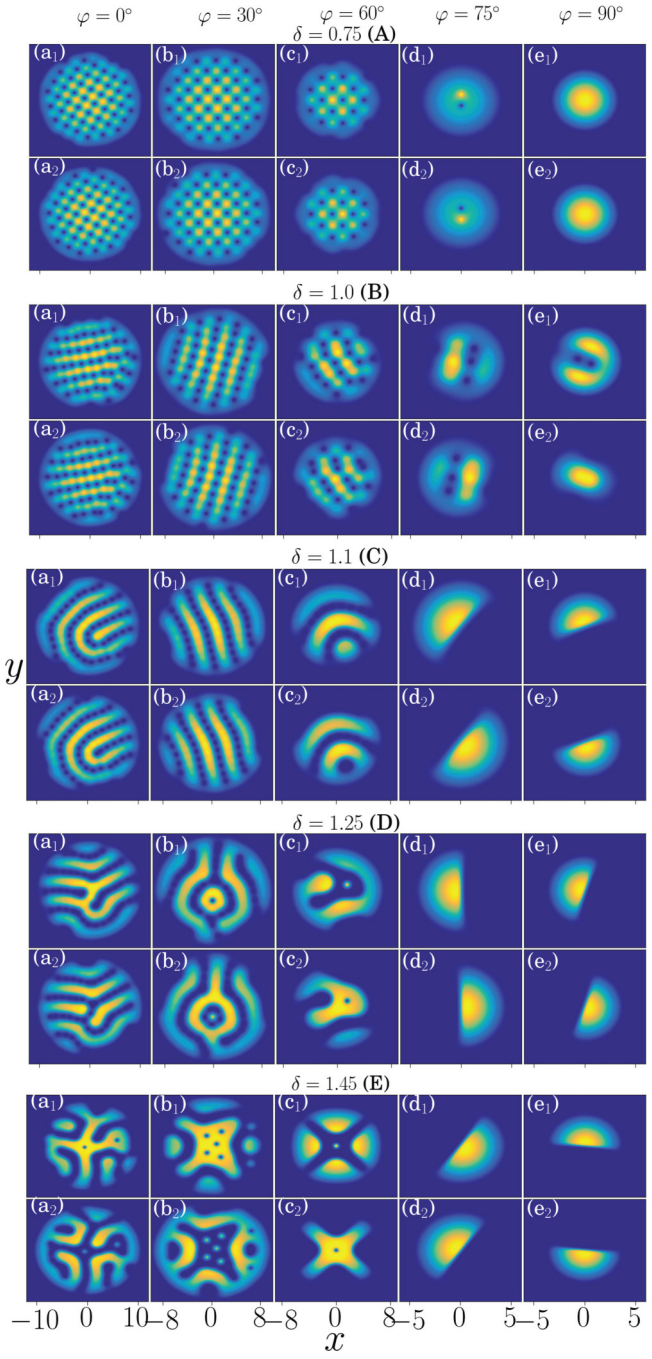

FIG. 2. The 2D densities $|\psi_{j=1,2}|^2$ are shown for the ^{164}Dy-^{162}Dy dipolar mixture ($j = 1$ is the ^{164}Dy, with $j = 2$ the ^{162}Dy), by tuning the polarization angle φ from 0° [(a_j)] to 90° [(e_j)], with δ varying from 0.75 [set (A)] to 1.45 [set (E)]. All panels have square formats, with y labels being the same as the indicated x labels. The (x, y) and $|\psi_j|^2$ are dimensionless, with $l_\perp = 1$ μm being the space unit. The density levels vary from 0 (darker) to a limit ranging $0.009 \sim 0.12$ (lighter), fixed to 1 by their respective normalization.

(a_j)–(c_j) of Fig. 2(A)]. By further increasing φ, a single vortex is verified at $\varphi = 75^\circ$, which disappears at $\varphi = 90^\circ$, when the assumed rotation ($\Omega = 0.6$) was verified not to be enough to form visible vortices. So, the miscibility of the coupled system becomes almost complete ($\eta \approx 1$) at $\varphi \sim 90^\circ$, with

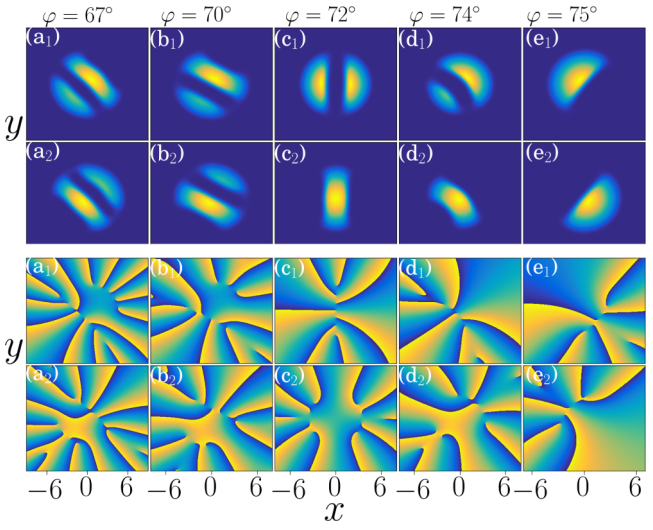

FIG. 3. 2D densities $|\psi_{j=1,2}|^2$ are shown in the upper two sequences of panels, for the ^{164}Dy-^{162}Dy mixture, as in Fig. 2(C) ($\delta = 1.1$), but considering the tuning-polarization angle from 67° [(a_j)] to 75° [(e_j)]. In the lower two sequences of panels, we have the respective diagrams for the phases, changing from $-\pi$ (darker) to $+\pi$ (lighter), with hidden vortices being confirmed. All panels have square formats, with y labels being as the indicated x labels. The (x, y) and $|\psi_j|^2$ are dimensionless, with space unit $l_\perp = 1$ μm.

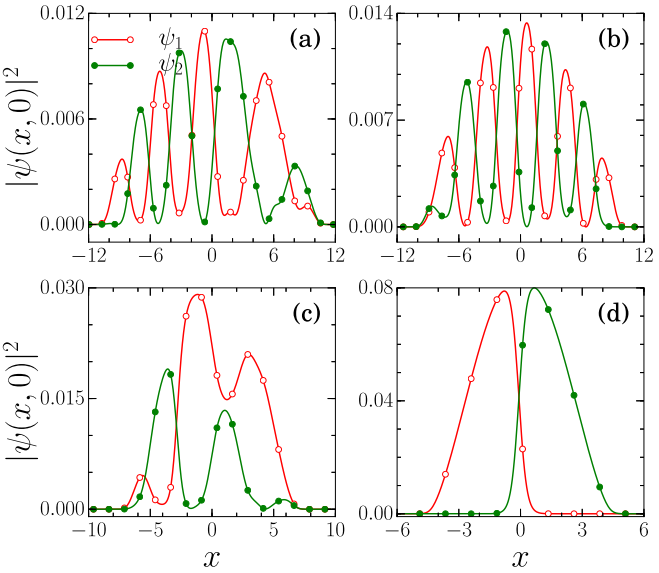

FIG. 4. Two-component ($j = 1, 2$) densities for the binary mixture ^{164}Dy-^{162}Dy as functions of x with $y = 0$, corresponding to $\delta = 1.1$ [2(C)], for the polarization angles $\varphi = 0°$ (a), 30° (b), 60° (c), and 75° (d). In particular, panel (d) shows the mixture reaching an almost complete spatial separation of the densities. All quantities are dimensionless, with space unit $l_\perp = 1$ μm.

the coupled system being dominated by the attractive dipolar forces in a miscible regime of the inter- to intraspecies contact interactions.

For $\delta = 1$ (the condition for MIT in homogeneous system), the effect of tuning the dipoles by increasing φ is similar to the case with $\delta < 1$ for repulsive DDI. For the attractive region of DDI, with $\varphi \geqslant 60°$, one can verify the appearance of double-core vortices, being reduced to a single double core for each species as φ moves near 90°.

When already in the immiscible regime ($\delta > 1$), by increasing φ the dipolar interaction becomes less repulsive, changing to attractive for $\varphi > 54.7°$. In this situation, the sizes of the coupled condensates are reduced, with the number of vortices decreasing, leading to a complete spatial separation of both components at some critical large angle $\varphi \sim 75°$, a regime dominated by attractive dipolar and repulsive contact interactions.

As the dipolar mixture is symmetric, the spatial separation turns out to be angular and not radial. The almost complete spatial separation in the attractive part of the dipolar interaction is verified in sets (C), (D), and (E) of Fig. 2 ($\delta = 1.1$, 1.25, and 1.45, respectively) when the polarization angle $\varphi \geqslant 75°$. The domain-wall vortex patterns verified with $\delta = 1.25$ and 1.45 when $\varphi = 0$ and 30° start changing as the interaction becomes attractive, at $\varphi = 60°$, until we have the almost complete spatial separation at some critical angle φ_c.

Before that, at some intermediate angles $\varphi < \varphi_c$, it is possible to observe rotating dropletlike states, as we can verify particularly in panels (a_j)–(c_j) of Fig. 2(E). These kinds of rotating dropletlike structures have already been observed in Ref. [39] when considering particular values of δ and rotation angles Ω. Due to the immiscibility, rotating droplet density peaks are formed near the surface of the first component, being located near the middle of the condensate for the second component. In the structures of the rotating droplets' vortex lattice, we observe about vorticity 2 in the small-sized ones and about 4 in the large-sized ones. They are similar as in the case of double-core structures, with rotating droplets in any one of the components being formed by multiple vortices with the same circulation. For the rotation frequency we are using, $\Omega = 0.6$, we notice that the condition for producing these rotating droplets is found to be for interactions given by $\delta = 1.45$ and $\varphi = 30°$, as represented in the panels (b_j) of Fig. 2(E). By φ, as exemplified in panels (c_j) of Fig. 2(E) (when $\delta = 1.45$), these rotating droplets are suppressed, with the number of vortices being reduced due to the attractive contributions in the DDI.

Half-space angular separation. In order to verify more closely how the spatial separation occurs in this symmetric-dipolar mixture, we consider $\delta = 1.1$, with the polarization angles varying close to some critical value where we can define the existence of an almost complete spatial separation. We can concentrate our discussion on the spatial separation to this value of δ, considering that for larger values of this parameter one can observe from Fig. 2 that the half-space angular separation is quite similar. For that, we provide Figs. 3 and 4. In Fig. 3, we show a set of panels with the densities and the corresponding phase diagrams for the vortex states by considering φ varying from 67° to 75°. With these panels, we show how we define the critical angles. As we increase φ in this interval, we observe that the initial two maxima verified for $\varphi = 67°$, for each component, reduce to just one maxima when $\varphi = \varphi_c = 75°$, as in the panels (d_j) of Fig. 2(C). (For $\varphi = 74°$ we can still observe two maxima in the densities of one of the components.) The densities for the coupled mixture are further analyzed with the one-dimensional plots ($y = 0$)

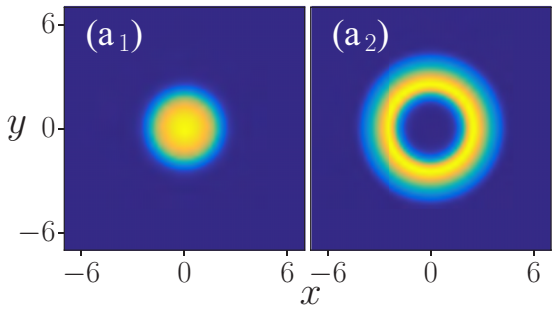

FIG. 5. Nonrotating ($\Omega = 0$) condensate densities for the dipolar mixture ^{164}Dy-^{162}Dy, considering $\delta = 1.1$ and $\varphi = 75°$, corresponding to panels (d_j) of Fig. 2(C). All quantities are dimensionless, with space unit $l_\perp = 1\ \mu$m.

shown in Fig. 4 for $\varphi = 0°, 30°, 60°$, and $75°$, where the almost complete spatial separation is observed at Fig. 3(d).

The immiscibility increases with the dominance of the interspecies contact interactions (repulsive) relative to the corresponding dipolar interactions (attractive). At the same time, with the dipolar interactions being more attractive as φ increases, with identical strengths, $d_{11} = d_{22}$, the spatial distribution of both condensates is reduced with the same proportion. So, without rotation, the only relevant parameter is the mass difference between the species, such that the corresponding densities should be distributed radially, with the more massive one at the center, as seen in Fig. 5. Under rotation, the maxima for the densities are shifted symmetrically from the center, as seen in panel (d) of Fig. 4 for $\delta = 1.1$, determined by dipolar symmetry of the mixture and the vorticity. We should observe that the effect of small mass difference (shown to be relevant when $\delta = 1$) is almost suppressed in this rotating immiscible regime.

Role of hidden vortices. In order to modify the nonrotating distribution seen in Fig. 5 to that particular half-space distribution, when the rotation frequency is switched on with $\Omega = 0.6$, one should expect the occurrence of vortices in both coupled condensates, which should contribute to the separability of the species. In fact, the existence of vortices not visible in the density distribution are evidenced at the low-density regions by the phase diagrams shown in Fig. 3 (lower two set of panels) for φ close to the almost complete spatial separation. Such "hidden vortices" have been studied in Ref. [40], where they are clarifying that they can be revealed in the free expansion of the condensate.

Related to hidden vortices, we should also consider the Feynman's rule derived within a TF approximation for a single condensate [41], predicting the total number of vortices (generated by a given rotation frequency) as given by $N_v \approx 2\Omega\langle x^2\rangle$ (considering our dimensionless units in a quasi-2D spherically symmetric condensate). This is approximately verified in our case for a complete repulsive system ($\varphi = 0$) by counting the visible vortices for each component. As moving to attractive DDI (higher polarization angles), fewer vortices are visible than the predicted one. The "puzzling" absence of visible vortices (expected from the use of Feynman's rule) in a specific case of rotating trapped condensate was previously reported in the Fetter review [41]. The core size of a visible vortex

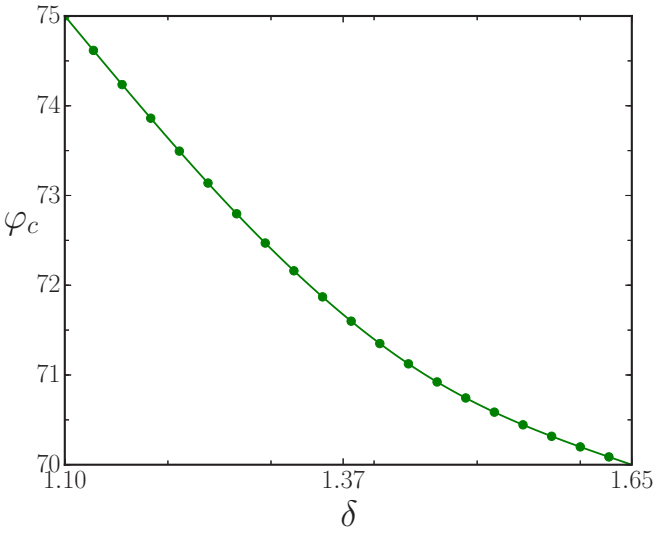

FIG. 6. Critical angle φ_c (in degrees) for the almost complete spatial separation of the mixture ^{164}Dy-^{162}Dy, considering the relevant interval region of δ that we are studying.

is about the healing length, which goes as the square root of the inverse of the original local density (without vortices). The hidden vortices are located at very small density regions but have their core sizes determined by the barrier width not by the healing length (as occurs for "ghost vortices" [42]). Therefore, they can contribute to the angular momentum, with Feynman's rule being well satisfied only after summing these vortices. This was discussed in Ref. [40] by using rotating system with double-well potential, where they pointed out that hidden vortices should also occur with other external potentials in condensed systems. The validity of Feynman's rule was also confirmed in Refs. [43,44] only after including the verified hidden vortices. In nonhomogeneous dipolar BEC, the hidden vortices are also verified to contribute to the separability of the condensate in Ref. [45] for 3D repulsive dipolar interactions with different rotation frequencies.

For the almost complete spatial separation of the ^{164}Dy-^{162}Dy mixture, the corresponding critical angle φ_c is estimated for several values of $\delta > 1$, with the results shown in Fig. 6. This angle decreases from 75° to 70° as δ varies, respectively, from 1.1 to 1.65. By increasing δ in this interval, the system becomes less miscible, with the spatial separation being reached for smaller values of φ. Therefore, the kind of angular spatial separation which emerges at smaller polarization angles (less attractive DDI) as δ increases appears when the interspecies repulsive forces (contact interactions together with hidden vortices) become the dominant ones.

In this dipolar-symmetric case, the miscibility should be affected in the same way as in the case of nondipolar systems when applying the homogeneous condition (8), considering that all the inter- and intraspecies interaction terms are modified by the same dipolar factor, which provides more repulsion or attraction to the system. By increasing δ we provide more repulsion between the interspecies, implying that the system becomes less miscible (decreasing η). This effect is clearly shown by the five different curves presented in Fig. 7 when we assume the polarization angle φ is fixed. In fact, as seen

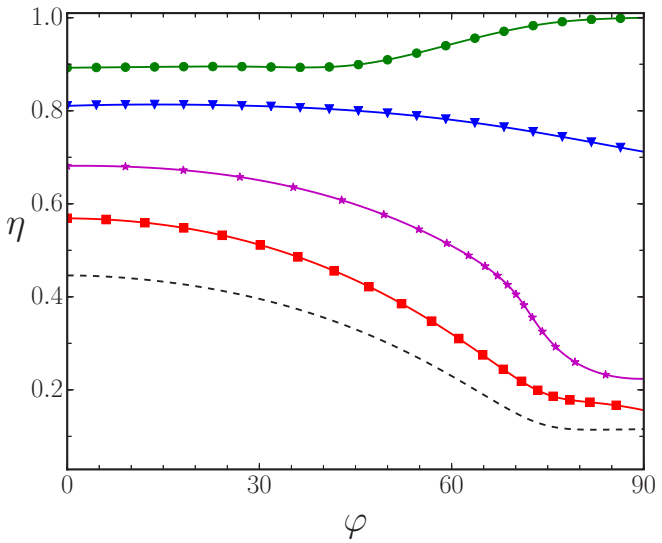

FIG. 7. The miscibility parameter (η), defined in Eq. (9), is given as a function of the polarization angle φ (in degrees) for the five cases of inter- to intraspecies contact interactions shown in Fig. 2. For $\delta = 0.75$, we have the green-solid line with circles; for $\delta = 1.0$, the blue-solid line with triangles; for $\delta = 1.1$, the purple-solid line with stars; for $\delta = 1.25$, the red-solid line with squares; and for $\delta = 1.45$ the dashed line.

in Fig. 7, the main miscibility behavior given by δ remains when we vary φ from zero to 54.7°, the point where the DDI is reduced to zero. By further increasing φ, we have the interspecies repulsive effect due to δ being diminished as the attractive intraspecies DDIs increase, which helps the system to become less immiscible. This behavior is clearly seen in the case that $\delta < 1$ (upper green line with bullets in Fig. 7), when the attractive effect due to DDI is dominant in comparison with repulsive effects due to interspecies contact interactions. However, for $\delta > 1$, the coupled system is shown to become less miscible when the polarization angle is $\varphi \geqslant \varphi_c$, besides the attraction provided by the DDI, which is still effective as verified in Fig. 2 by the shrinking of the radius. However, for the miscibility, the main roles are provided by the interspecies interactions. As the system becomes less miscible for $\varphi \geqslant \varphi_c$, we conclude that the repulsive interspecies contact interactions are dominant in this region where the DDI is attractive. The combination of both of the effects (one due to repulsive contact interactions, reducing the miscibility; the other due to attractive DDI, reducing the spatial size of the condensates) results in the observed half-space spatial separation of the mixture for $\varphi \geqslant 75°$, where hidden vortices have also been identified due to the rotation, as we have discussed with Figs. 3 and 4.

Role of mass symmetry. This symmetric-dipolar case is appropriate to verify a striking result due to the mass-symmetry breaking, in rotating systems, represented by the set with $\delta = 1$ in Fig. 2(B). We should note that by considering the hypothetical case that $m_2 = m_1$ in Eqs. (3) and (4), the coupled two-component equation reduces to a single-component one, implying that the results for the densities presented in the upper and lower panels of Fig. 2(B) should be identical, with the vortices due to the rotation occurring at the same position. This is confirmed by our numerical solution for the coupled system Eq. (4) with $m_1 = m_2$. Therefore, the results shown in Fig. 2(B) (when $\delta = 1$ and $m_1 \neq m_2$) are basically reflecting the mass asymmetry in the densities. We found quite remarkable that such observed differences between the upper and corresponding lower panels of Fig. 2(B) (in particular, for the cases when $\varphi > \varphi_M$) correspond to such quite small mass asymmetry, $m_1/m_2 - 1 = 1/81$, which appears explicitly in the second kinetic-energy term of the coupled Eq. (4). However, this is consistent with our explanation presented in the Sec. III for the miscibility, justifying the estimation of the miscibility of nonhomogeneous binary mixtures by using η, defined in Eq. (9).

Structure of the patterns. For the structure and boundary domains of stripes presented in binary mixtures, one can follow the analysis provided in Ref. [46], where an approximate TF profile was used, considering that the only nonlinear repulsive forces in a rotating coupled system are due to contact interactions. This analysis was restricted to the symmetric case with $\delta = 1$, when all the masses and frequencies and number of atoms are identical for both species, being quite approximate for $\delta > 1$. In our case, the corresponding behavior can be followed from the results shown by (a_i)–(c_i) of Fig. 2 for fixed repulsive DDI, when the TF approach can still be approximately valid. As shown, the stripes become larger by increasing δ, changing to serpentinelike and domain-wall patterns. Correspondingly, one could try to transfer the analysis performed in Ref. [46] to the cases where we modify the DDI (varying φ for fixed δ). However, in this case an apparent different behavior is verified. As shown in Fig. 2(C), for example, the stripes become wider when the DDI becomes more attractive. In order to explain that, we first should observe that the TF approximation is not applicable for attractive interactions, such that it becomes less valid as we increase the angle φ. Next, we notice that both interactions (contact and dipolar) are not being varied in the same way. When we vary the DDI by tuning the dipoles, all the inter- and intraspecies are being changed in the same way such that the ratio between inter- and intraspecies dipolar interaction remains fixed, whereas when changing δ only the interspecies interactions are being modified. Therefore, the observed increasing in the width of the stripes as the DDI turns out to be more attractive is an effect due to the fact that the condensates are shrinking, reducing the space of the overlap between the two species. From one side, by increasing δ, the system becomes less miscible, and from the other side, the coupled condensates are shrinking by increasing the DDI. Together, the interplay of these two effects will result in an almost complete spatial separation between the densities, as observed in Fig. 2 for $\varphi \geqslant 75°$ with $\delta > 1$. A critical angle φ_c can be defined in this case as being given by the condition that the densities of both species have well defining two maxima, one for each species. This kind of separation that occurs in the immiscible phase ($\eta < 0.35$) for symmetric-dipolar mixtures we call "angular spatial separation." As it will be shown, for the immiscible phase of the asymmetric cases, the spatial separations will be radial instead of angular.

Resuming our results for the ^{164}Dy-^{162}Dy binary mixture, we have studied the anisotropic effects due to dipolar interactions by tuning the orientation angle of dipoles from

miscible to immiscible cases. The fundamental vortex-lattice structures which occur for repulsive dipolar interactions ($\varphi < 54.7^\circ$) remain until the attractive dipolar interactions become dominant with respect to the inter- to intraspecies contact interactions.

B. The asymmetric-dipolar mixture, ^{168}Er-^{164}Dy

Here we discuss anisotropic effects of dipolar interactions for the asymmetric ^{168}Er-^{164}Dy mixture by considering particular characteristics which distinguish asymmetric mixtures from the symmetric ones. From previous analysis [29], we understand that the vortex-lattice patterns for repulsive dipolar DDI mainly feature triangular, squared, and circular vortex-lattice structures in this binary mixture. This asymmetric-dipolar mixture is less miscible than the symmetric-dipolar case due to the imbalances of dipole moments and masses of the two species. Even when $\delta < 1$ it is less miscible and we have dominant repulsive interspecies DDI with $\varphi \leqslant \varphi_c$. The heavier mass ^{168}Er component remains mainly distributed in the center, surrounded by the lighter mass one, ^{164}Dy. In general, for repulsive DDI, this behavior remains similar for $\delta > 1$, as can be seen in Fig. 8. Such a result can first be understood when considering the homogeneous condition (8), because the dipolar asymmetry is modifying the point where one should expect the MIT, from $\delta = 1$ (dipolar-symmetric case) to $\delta < 1$ (dipolar-asymmetric case). This effect due to the dipolar interactions becomes quite clear when we consider a polarization angle close to the magic angle $\varphi_c = 54.7^\circ$, where the system is nondipolar. For example, in Fig. 8 one can see how the patterns vary as we increase δ for the case where we have $\varphi = 60^\circ$, compared with other cases. So, by increasing φ we are reducing the repulsive effect due to interspecies contact interactions, with the transition point being accordingly modified. However, in view of the mass asymmetry it is more reliable to consider Eq. (9) to estimate the miscibility of this rotating coupled dipolar system. We should notice that the dipolar asymmetry together with the mass differences of the two species are relevant to explain the observed pattern distributions.

By tuning the polarization angle and increasing φ, the DDI becomes attractive, providing the imbalanced dipolar counterpart. For example, the ^{168}Er has a lower magnetic moment than the ^{164}Dy, implying that ^{164}Dy will have a larger attractive dipolar interaction than the ^{168}Er. This will affect the corresponding radial sizes of the components in the mixture, with ^{164}Dy shrinking more than ^{168}Er. The corresponding density distributions, observed for the components in Fig. 8, clearly indicate this general behavior in all the sets, with different values for the contact interactions, by the exchange positions between inner and outer components, as the dipole interactions change from repulsive to attractive. For $\varphi \geqslant 75^\circ$ [panels (d_j) of Fig. 8], we observed that the ^{164}Dy component is already surrounded by the ^{168}Er one, implying a radial spatial separation, which becomes more pronounced for $\delta \geqslant 1$. This is expected from previous studies, as a binary mixture becomes less miscible by increasing the repulsive interspecies contact interactions [28,29].

With Fig. 9 we present our results for the behavior of the miscibility of this asymmetric mixture, ^{168}Er-^{164}Dy, with respect to the changes in the polarization angle for each of the sets of δ shown in Fig. 8. In this case, for all the sets we observe a similar behavior of η with respect to φ, with the coupled system becoming more miscible when increasing φ until some critical angle where the miscibility reaches a maximum. The behavior for the smaller angles differs from

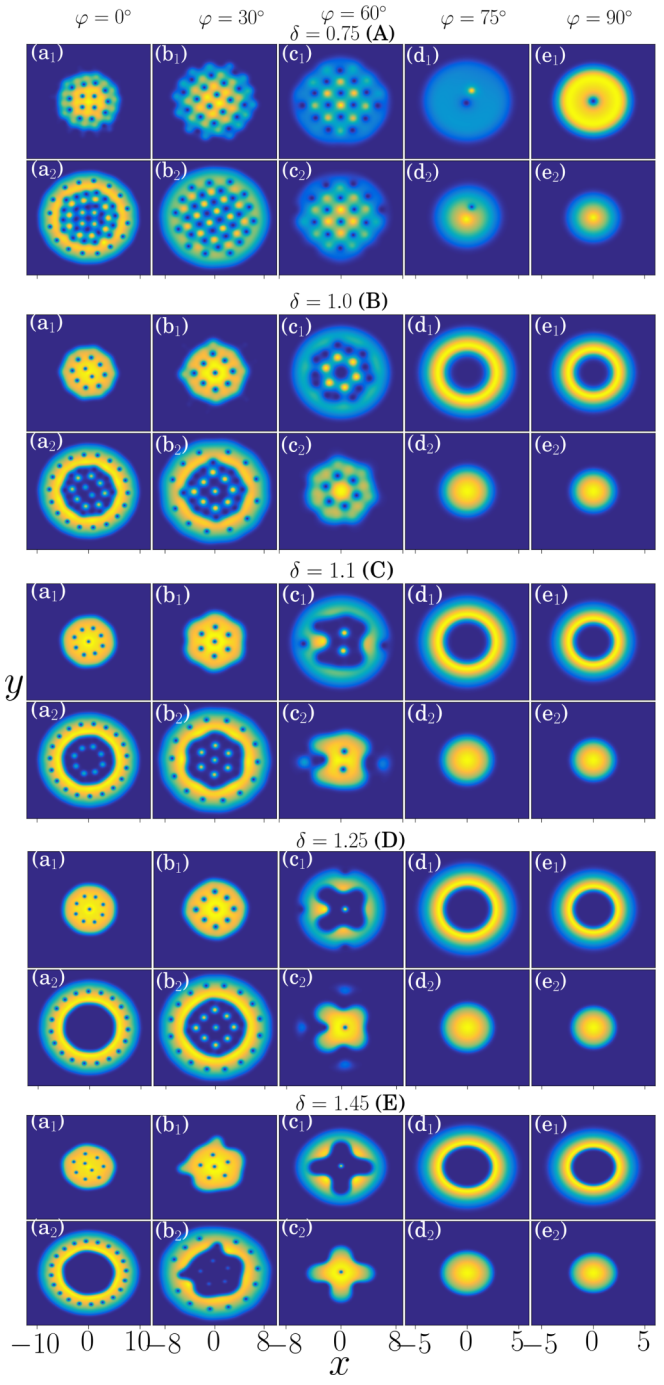

FIG. 8. The 2D densities $|\psi_{j=1,2}|^2$ are shown for the ^{168}Er-^{164}Dy dipolar mixture ($j = 1$ is the ^{168}Er, with $j = 2$ the ^{164}Dy), by tuning φ from 0 [(a_j) panels] to 90° [(e_j) panels], with δ varying from 0.75 [set (A)] to 1.45 [set (E)], as in Fig. 2. All panels have square formats, with y labels being the same as the indicated x labels. All quantities are dimensionless, with space unit $l_\perp$. The density levels vary from 0 (darker) to a limit ranging 0.01 ∼ 0.105 (lighter), fixed by their respective normalization to 1.

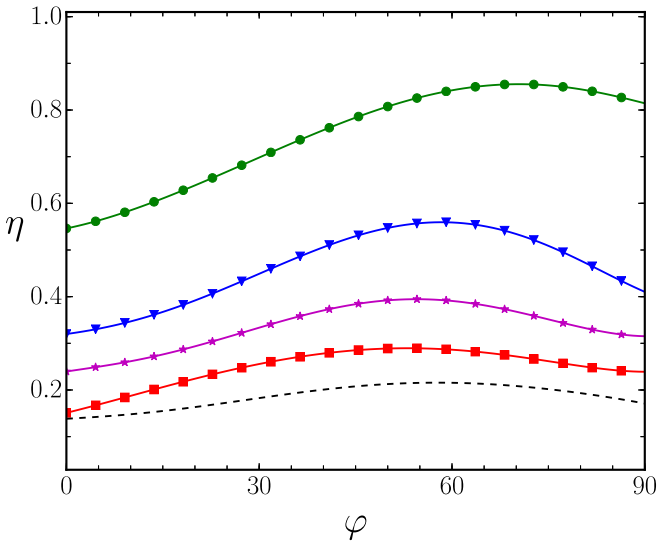

FIG. 9. Miscibility of the dipolar mixture ^{168}Er-^{164}Dy, defined by η, as a function of the polarization angle φ (in degrees). For $\delta = 0.75$, we have the green-solid line with circles; for $\delta = 1.0$, the blue-solid line with triangles; for $\delta = 1.1$, the purple-solid line with stars; for $\delta = 1.25$, the red-solid line with squares; and for $\delta = 1.45$, the dashed line.

those verified in Fig. 7 (where η is not increasing in this interval with $\varphi < 54.7^\circ$). The system ^{168}Er-^{164}Dy is less miscible for $\varphi = 0^\circ$, with the miscibility increasing as the DDI becomes less repulsive. For larger polarization angles, we have the combined effect of attractive DDI (reducing the radius and increasing η) together with the repulsive contact interactions until a maximum at some critical φ_c, where there is a balance between the two combined effects. For $\varphi \geqslant \varphi_c$, the contact interactions start to become dominant in relation to the DDI. As observed in Fig. 9, the critical angles are in a small interval, being $\sim 70^\circ$ for $\delta = 0.75$, $\sim 60^\circ$ for $\delta = 1$, and $\sim 55^\circ$ to ~ 60 for $\delta =$ between 1.1 and 1.45. Next, for $\varphi > \varphi_c$, as observed in Fig. 8, the system starts to become less miscible with the emergence of a radial spatial separation, which differs from the dipolar-symmetric case where the corresponding separation is angular.

C. The asymmetric-dipolar mixture, ^{164}Dy-^{87}Rb

The binary mixture ^{164}Dy-^{87}Rb is more asymmetric with respect to the dipolar magnetic moments of each component that the other cases that we have considered, with the magnetic moment of ^{87}Rb being almost negligible, such that the effect of the polarization angle is less effective, as due mostly to the ^{164}Dy component. In this case, the rubidium component of the mixture is more concentrated in the center when considering the region where the DDI is more repulsive (as shown in Fig. 10 for $\varphi = 0$ and 30°), with the dysprosium component distributed within a larger radius. The results are quite similar for the three sets of δ that we are examining. When the DDI changes to an attractive one, as verified for $\varphi \geqslant 60^\circ$, we observe an interplay between the distributions of the two components, with the radius of the ^{164}Dy (component $j = 1$) being strongly reduced in relation to the radial distribution

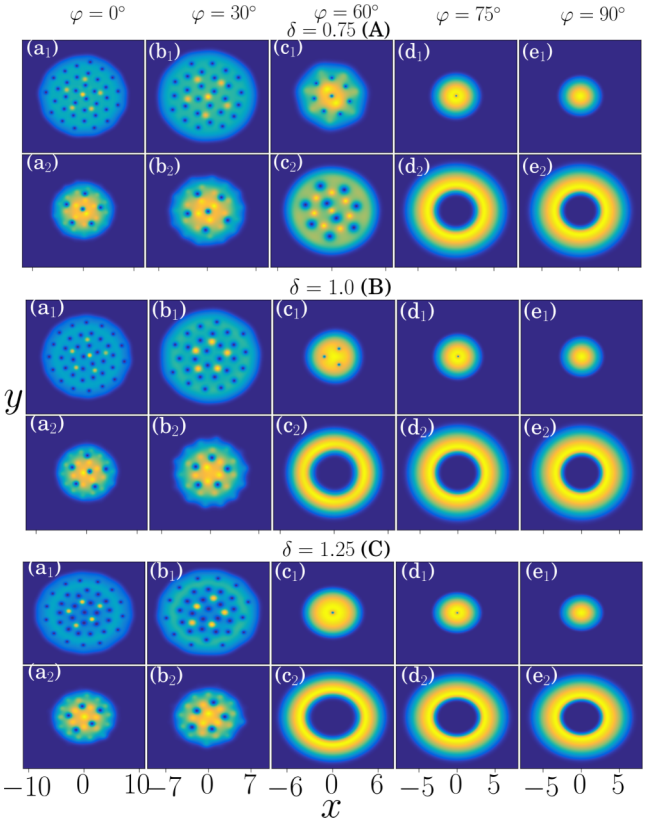

FIG. 10. The 2D densities $|\psi_{j=1,2}|^2$ for the ^{164}Dy-^{87}Rb dipolar mixture ($j = 1$ is the ^{164}Dy, with $j = 2$ the ^{87}Rb) by tuning the polarization angle φ from 0° [(a_j) panels] to 90° [(e_j) panels] for $\delta = 0.75$ [set (A)], 1.0 [set (B)], and 1.25 [set (C)]. As in Figs. 2 and 8, all panels have square formats such that only x labels are indicated, with corresponding sizes decreasing from left to right. All quantities are dimensionless, with space unit $l_\perp = 1$ μm. The density levels vary from 0 (darker) to a limit ranging 0.01 $\sim$ 0.08 (lighter), fixed by their respective normalization to 1.

of the ^{87}Rb ($j = 2$). As in the previous discussed mixture, of erbium and dysprosium, here also the effect is clearly due to the large differences between the magnetic moments of both species: the DDI is more attractive for the species with larger intraspecies magnetic moment, implying a smaller radial distribution. In particular, we notice that this behavior with the corresponding radial spatial separation is happening even for $\delta < 1$, when the DDI becomes attractive. This reflects the dominance of the attractive intraspecies DDI in relation to the repulsive effects due to the intraspecies contact interactions. Also, the radial separation is similar to that obtained for the ^{168}Er-^{164}Dy mixture, when the DDI is attractive, with $\delta \geqslant 1$.

One characteristic of this mixture can be observed when φ is near 60°, which is close to the polarization "magic angle" $\varphi_M = 54.7^\circ$, where the DDI is zero. The results obtained for panels (c_j) are expected to correspond to the results presented in panels (c_j) of Fig. 8, if the mass differences were the same. However, in the present case, the mass of the second species, the rubidium, is about half of the dysprosium. So the results shown a more clear separation between the species, which can only be explained by the mass differences, together with the larger difference in the magnetic moments.

V. SUMMARY AND CONCLUSION

The polarization of the dipoles is found instrumental in the process of tuning the dipolar interactions from repulsive to attractive, by considering three different rotating coupled mixtures. With the dipoles of the two species polarized in the same direction, perpendicular to the direction of the dipole alignment ($\varphi = 0$), the DDI is repulsive. By tuning the polarization angle φ from zero to 90° the DDI changes from repulsive to fully attractive. The miscibility of the condensed mixture is mainly affected by the interspecies interactions, with the vortex-pattern structures being related to combined effects due to inter- and intraspecies interactions. The vortex-pattern formations obtained with $\varphi = 0$ (repulsive DDIs) survive approximately up to some angle at which the DDIs become attractive.

One of the main outcomes of the present study is verified by the almost complete spatial separation in the two-component densities under rotation, which occurs for large polarization angles, when the DDI is attractive. We have verified half-space angular separations of the densities in the case of a dipolar-symmetric mixture, represented by ^{164}Dy-^{162}Dy, whereas the separations have radial space distribution for the dipolar-asymmetric cases, represented by ^{168}Er-^{164}Dy and ^{164}Dy-^{87}Rb. For $\delta > 1$ (immiscible regime) and large polarization angle (attractive DDI), we determine the critical polarization angle where the symmetry is broken, leading to the occurrence of an almost complete spatial separation of the mixture. As shown, the number of vortices and miscibility of the binary mixtures are significantly affected by the polarization angle, with the dipolar attraction being relevant to reduce the spatial distribution of both condensates, by merging vortices together. For the symmetric-dipolar case, when the spatial separation is almost complete, as the intraspecies dipolar interactions are identical, the positions for the maxima of both densities are at the same distance from the center, resulting in an angular half-space separation. For the nonrotating regime, only the small mass asymmetry is relevant for the observed radial positions of the condensates, as verified. For the asymmetric-dipolar case, the almost complete spatial separation is radial, which can be explained by the intraspecies attractive interactions of both species such that a species with larger magnetic moment will have a smaller radius, being at the center. In the nonrotating regime, the mass differences of the asymmetric-dipolar coupled species considered are not enough to alter this kind of configuration.

Also related to the particular rotating symmetric-dipolar case, as an unexpected outcome, we have verified the appearance of hidden vortices in the observed structure of the spatial separation which occurs for attractive DDI. Further investigations are suggested on the role of hidden vortices in rotating coupled BEC systems, by varying the rotation and nonlinear parameters.

Another quite relevant result is the observed effect of the mass asymmetry in the miscibility and vortex-pattern structures. The particular mass-imbalance sensitivity can first be appreciated by considering the dipolar-symmetric mixture ^{164}Dy-^{162}Dy for $\delta = 1$, when all the differences between the density patterns of the two species should be attributed to the mass asymmetry. Therefore, one should consider a more general condition for the MIT than that derived for homogeneous systems, such as the one given by Eq. (9), where the asymmetries in the linear terms (kinetic energy or external trap) can be taken into account by the densities. By examining the corresponding case with $\delta = 1$ for the dipolar-asymmetric mixtures, one should also expect similar density patterns for the two species if applying the homogeneous condition for the MIT. However, the system is already less miscible than the dipolar-symmetric case for $\delta < 1$. In this case, we have combined effects of the imbalanced masses and dipolar interactions. For a given value of δ, as the DDI changes from repulsive to attractive, the two species exchange their position radially. Located in a small radius at the center we have the species with a higher magnetic moment, for attractive DDI. Otherwise, for repulsive DDI, the weaker dipolar species will be at the center. The effect of mass differences in these dipolar-asymmetric cases can be verified by the nonhomogeneous miscibility condition when comparing the results with the dipolar-symmetric case.

ACKNOWLEDGMENTS

The authors thank the Brazilian agencies Fundação de Amparo à Pesquisa do Estado de São Paulo (FAPESP) [Contracts No. 2014/01668-8(R.K.K.), No. 2016/14120-6(L.T.), and No. 2016/17612-7 (A.G.)] and Conselho Nacional de Desenvolvimento Científico e Tecnológico (CNPq) [153522/2018-6 (R.K.K.), 306191/2014-8 (L.T.), 304468/2014-2 (A.G.)] for partial support. L.T. is also partially supported by Coordenação de Aperfeiçoamento de Pessoal de Nível Superior (CAPES).

[1] A. Griesmaier, J. Werner, S. Hensler, J. Stuhler, and T. Pfau, Bose-Einstein Condensation of Chromium, Phys. Rev. Lett. **94**, 160401 (2005); A. Griesmaier, J. Stuhler, and T. Pfau, Production of a chromium Bose-Einstein condensate, Appl. Phys. B **82**, 211 (2006); T. Lahaye, C. Menotti, L. Santos, M. Lewenstein, and T. Pfau, The physics of dipolar bosonic quantum gases, Rep. Prog. Phys. **72**, 126401 (2009).

[2] T. Lahaye, T. Koch, B. Froehlich, M. Fattori, J. Metz, A. Griesmaier, S. Giovanazzi, and T. Pfau, Strong dipolar effect in a quantum ferrofluid, Nature (London) **448**, 672 (2007).

[3] M. Lu, S. H. Youn, and B. L. Lev, Trapping Ultracold Dysprosium: A Highly Magnetic Gas for Dipolar Physics, Phys. Rev. Lett. **104**, 063001 (2010); M. Lu, N. Q. Burdick, and B. L. Lev, Quantum Degenerate Dipolar Fermi Gas, *ibid.* **108**, 215301 (2012).

[4] K. Aikawa, A. Frisch, M. Mark, S. Baier, A. Rietzler, R. Grimm, and F. Ferlaino, Bose-Einstein Condensation of Erbium, Phys. Rev. Lett. **108**, 210401 (2012).

[5] L. Chomaz, R. M. W. van Bijnen, D. Petter, G. Faraoni, S. Baier, J. H. Becher, M. J. Mark, F. Wächtler, L. Santos, and F. Ferlaino,

Observation of roton mode population in a dipolar quantum gas, Nat. Phys. **14**, 442 (2018).

[6] J. Ulitzsch, D. Babik, R. Roell, and M. Weitz, Bose-Einstein condensation of erbium atoms in a quasielectrostatic optical dipole trap, Phys. Rev. A **95**, 043614 (2017).

[7] J. H. Becher, S. Baier, K. Aikawa, M. Lepers, J.-F. Wyart, O. Dulieu, and F. Ferlaino, Anisotropic polarizability of erbium atoms, Phys. Rev. A **97**, 012509 (2018).

[8] C. Ravensbergen, V. Corre, E. Soave, M. Kreyer, S. Tzanova, E. Kirilov, and R. Grimm, Accurate Determination of the Dynamical Polarizability of Dysprosium, Phys. Rev. Lett. **120**, 223001 (2018).

[9] V. Veljić, A. R. P. Lima, L. Chomaz, S. Baier, M. J. Mark, F. Ferlaino, A. Pelster, and A. Balaž, Ground state of an ultracold Fermi gas of tilted dipoles in elongated traps, New J. Phys. **20**, 093016 (2018).

[10] A. Trautmann, P. Ilzhöfer, G. Durastante, C. Politi, M. Sohmen, M. J. Mark, and F. Ferlaino, Dipolar Quantum Mixtures of Erbium and Dysprosium Atoms, Phys. Rev. Lett. **121**, 213601 (2018).

[11] P. Ilzhöfer, G. Durastante, A. Patscheider, A. Trautmann, M. J. Mark, and F. Ferlaino, Two-species five-beam magneto-optical trap for erbium and dysprosium, Phys. Rev. A **97**, 023633 (2018).

[12] E. Lucioni, L. Tanzi, A. Fregosi, J. Catani, S. Gozzini, M. Inguscio, A. Fioretti, C. Gabbanini, and G. Modugno, Dysprosium dipolar Bose-Einstein condensate with broad Feshbach resonances, Phys. Rev. A **97**, 060701(R) (2018).

[13] Y. Tang, W. Kao, K.-Y. Li, and B. L. Lev, Tuning the Dipole-Dipole Interaction in a Quantum Gas with a Rotating Magnetic Field, Phys. Rev. Lett. **120**, 230401 (2018).

[14] Y. Cai, Y. Yuan, M. Rosenkranz, H. Pu, and W. Bao, Vortex patterns and the critical rotational frequency in rotating dipolar Bose-Einstein condensates, Phys. Rev. A **98**, 023610 (2018).

[15] I. Ferrier-Barbut, H. Kadau, M. Schmitt, M. Wenzel, and T. Pfau, Observation of Quantum Droplets in a Strongly Dipolar Bose Gas, Phys. Rev. Lett. **116**, 215301 (2016); M. Schmitt, M. Wenzel, F. Böttcher, I. Ferrier-Barbut, and T. Pfau, Self-bound droplets of a dilute magnetic quantum liquid, Nature (London) **539**, 259 (2016).

[16] L. Chomaz, S. Baier, D. Petter, M. J. Mark, F. Wächtler, L. Santos, and F. Ferlaino, Quantum-Fluctuation-Driven Crossover from a Dilute Bose-Einstein Condensate to a Macrodroplet in a Dipolar Quantum Fluid, Phys. Rev. X **6**, 041039 (2016).

[17] V. I. Yukalov, Dipolar and spinor bosonic systems, Laser Phys. **28**, 053001 (2018).

[18] A. M. Martin, N. G. Marchant, D. H. J. O'Dell, and N. G. Parker, Vortices and vortex lattices in quantum ferrofluids, J. Phys.: Condens. Matter **29**, 103004 (2017).

[19] L. Santos, G. V. Shlyapnikov, and M. Lewenstein, Roton-Maxon Spectrum and Stability of Trapped Dipolar Bose-Einstein Condensates, Phys. Rev. Lett. **90**, 250403 (2003).

[20] D. H. J. O'Dell, S. Giovanazzi, and C. Eberlein, Exact Hydrodynamics of a Trapped Dipolar Bose-Einstein Condensate, Phys. Rev. Lett. **92**, 250401 (2004).

[21] S. Yi and L. You, Trapped condensates of atoms with dipole interactions, Phys. Rev. A **63**, 053607 (2001); Expansion of a dipolar condensate, **67**, 045601 (2003).

[22] M. Asad-uz-Zaman and D. Blume, Modification of roton instability due to the presence of a second dipolar Bose-Einstein condensate, Phys. Rev. A **83**, 033616 (2011).

[23] H. Saito, Y. Kawaguchi, and M. Ueda, Ferrofluidity in a Two-Component Dipolar Bose-Einstein Condensate, Phys. Rev. Lett. **102**, 230403 (2009).

[24] K.-T. Xi, T. Byrnes, and H. Saito, H. Fingering instabilities and pattern formation in a two-component dipolar Bose-Einstein condensate, Phys. Rev. A **97**, 023625 (2018).

[25] X. Zhang, W. Han, L. Wen, P. Zhang, R.-F. Dong, H. Chang, and S.-G. Zhang, Two-component dipolar Bose-Einstein condensate in concentrically coupled annular traps, Sci. Rep. **5**, 8684 (2015).

[26] R. M. Wilson, C. Ticknor, J. L. Bohn, and E. Timmermans, Roton immiscibility in a two-component dipolar Bose gas, Phys. Rev. A **86**, 033606 (2012).

[27] X. F. Zhang, L. Wen, C.-Q. Dai, R.-F. Dong, H.-F. Jiang, H. Chang, and S.-G. Zhang, Exotic vortex lattices in a rotating binary dipolar Bose-Einstein condensate, Sci. Rep. **6**, 19380 (2016).

[28] R. K. Kumar, P. Muruganandam, L. Tomio, and A. Gammal, Miscibility in coupled dipolar and non-dipolar Bose-Einstein condensates, J. Phys. Commun. **1**, 035012 (2017).

[29] R. K. Kumar, L. Tomio, B. A. Malomed, and A. Gammal, Vortex lattices in binary Bose-Einstein condensates with dipole-dipole interactions, Phys. Rev. A **96**, 063624 (2017).

[30] R. K. Kumar, L. Tomio, and A. Gammal, Vortex patterns in rotating dipolar Bose-Einstein condensate mixtures with squared optical lattices, J. Phys. B: At. Mol. Opt. Phys. **52**, 025302 (2019).

[31] S. Inouye, M. R. Andrews, J. Stenger, H.-J. Miesner, D. M. Stamper-Kurn, and W. Ketterle, Observation of Feshbach resonances in a Bose-Einstein condensate, Nature (London) **392**, 151 (1998).

[32] C. Chin, R. Grimm, P. Julienne, and E. Tiesinga, Feshbach resonances in ultracold gases, Rev. Mod. Phys. **82**, 1225 (2010).

[33] S. Giovanazzi, A. Görlitz, and T. Pfau, Tuning the Dipolar Interaction in Quantum Gases, Phys. Rev. Lett. **89**, 130401 (2002).

[34] K. Góral and L. Santos, Ground state and elementary excitations of single and binary Bose-Einstein condensates of trapped dipolar gases, Phys. Rev. A **66**, 023613 (2002).

[35] R. K. Kumar, L. E. Young-S, D. Vudragović, A. Balaž, P. Muruganandam, and S. K. Adhikari, Fortran and C programs for the time-dependent dipolar Gross-Pitaevskii equation in an anisotropic trap, Comput. Phys. Commun. **195**, 117 (2015).

[36] M. Brtka, A. Gammal, and L. Tomio, Relaxation algorithm to hyperbolic states in Gross-Pitaevskii equation, Phys. Lett. A **359**, 339 (2006).

[37] C. J. Pethick and H. Smith, *Bose-Einstein Condensation in Dilute Gases* (Cambridge University Press, Cambridge, England, 2002).

[38] L. Wen, W. M. Liu, Y. Cai, J. M. Zhang, and J. Hu, Controlling phase separation of a two-component Bose-Einstein condensate by confinement, Phys. Rev. A **85**, 043602 (2012).

[39] K. Kasamatsu, M. Tsubota, and M. Ueda, Vortex Phase Diagram in Rotating Two-Component Bose-Einstein Condensates, Phys. Rev. Lett. **91**, 150406 (2003).

[40] L. Wen, H. Xiong, and B. Wu, Hidden vortices in a Bose-Einstein condensate in a rotating double-well potential, Phys. Rev. A **82**, 053627 (2010).

[41] A. L. Fetter, Rotating trapped Bose-Einstein condensates, Rev. Mod. Phys. **81**, 647 (2009).

[42] M. Tsubota, K. Kasamatsu, and M. Ueda, Vortex lattice formation in a rotating Bose-Einstein condensate, Phys. Rev. A **65**, 023603 (2002).

[43] S. Subramaniyan, Vortex formation and hidden vortices in dipolar Bose-Einstein condensates, Phys. Lett. A **381**, 3062 (2017).

[44] T. Mithum, K. Porsezian, and B. Dey, Pinning of hidden vortices in Bose-Einstein condensates, Phys. Rev. A **89**, 053625 (2014).

[45] R. K. Kumar, T. Sriraman, H. Fabrelli, P. Muruganandam, and A. Gammal, Three-dimensional vortex structures in a rotating dipolar Bose-Einstein condensate, J. Phys. B: At. Mol. Opt. Phys. **49**, 155301 (2016).

[46] K. Kasamatsu and M. Tsubota, Vortex sheet in rotating two-component Bose-Einstein condensates, Phys. Rev. A **79**, 023606 (2009).